Supplementary Data

Supplementary Table 1: Patient-level ROC curve analysis for the performance of FLT and fluorescence intensity in liver cancers

Patient ID	FLT			Intensity		
	Sensitivity	Specificity	AUC	Sensitivity	Specificity	AUC
P1	96.7	96	99.4	37.1	50	41.1
P2	97.9	98	99.8	96.8	94	98.9
P3	95.6	96	99.3	13.5	30	18.1
P4	90.1	96	97.1	48.8	30	36.1
P5	97.4	98	99.7	95.9	97	99.4
P6	100	99	99	14.6	30	13
P7	93	89	96.7	94.9	91	97.9
Mean ± SD	95.8±3.3	96±3.3	98.7±1.3	57.3±38.1	60.3±32.4	57.8±39.5

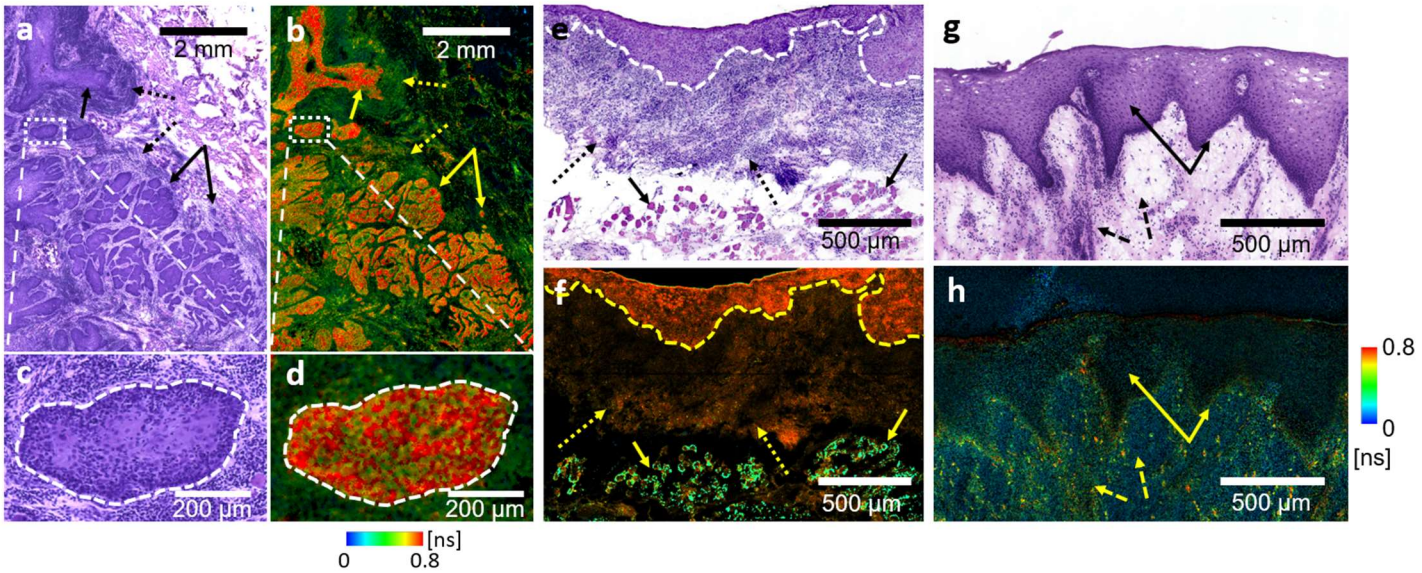

Fig. S1. Histology (**a**) and FLT (**b**) images of a tongue SCC specimen with ICG injection 20 h prior to surgery. Long FLT of ICG was observed to originate from the microscopic tumor nests (arrows) with short FLT components in the surrounding tissue. One such tumor cell nest (dotted rectangles in **a** and **b**) is shown with higher magnification in (**c**) (histology) and (**d**) (FLT). **c**, The tumor nest (dashed outline) can be identified at the center of the histology image within a matrix of desmoplastic stroma and lymphocytes (dotted arrow). **d**, Long FLT was observed only in the tumor nest while the desmoplastic stroma and lymphocytes showed short FLT (dotted arrow). **e**, Histology, and **f**, FLT images of a buccal SCC specimen with ICG injection 20 h prior to surgery. The tumor in the buccal epithelium can be identified by dashed lines in (**e**) and (**f**). The cancer cells clearly showed a longer FLT compared to the underlying muscle (solid arrows in (**e**) and (**f**)). The dotted arrows in (**e**) and (**f**) indicate tumor-infiltrating lymphocytes (TILs) with FLTs comparable to the tumor cells. **g**, Histology and **h**, FLT images of a normal oral epithelium showing low ICG uptake and short FLT across the epithelium (solid arrow) and the stroma (dashed arrow).

Supplementary Table 2: Patient-level ROC curve analysis for the performance of FLT and fluorescence intensity in HN cancer

Patient ID	FLT			Intensity		
	Sensitivity	Specificity	AUC	Sensitivity	Specificity	AUC
P1	99.7	98.7	0.99	96.5	94.3	0.98
P2	96.6	97.8	0.99	16.1	40.0	0.24
P3	100	92.3	0.99	35.5	80.6	0.53
P4	94.2	96.3	0.99	85.5	56.0	0.65
P5	97.2	94.6	0.97	65.7	58.9	0.69
P6	96.9	99.2	0.99	87.5	72.0	0.85
Mean ± SD	97.4±2.2	96.5±2.6	98.6±1	64.5±32.2	66.9±19.3	65.7±25.8

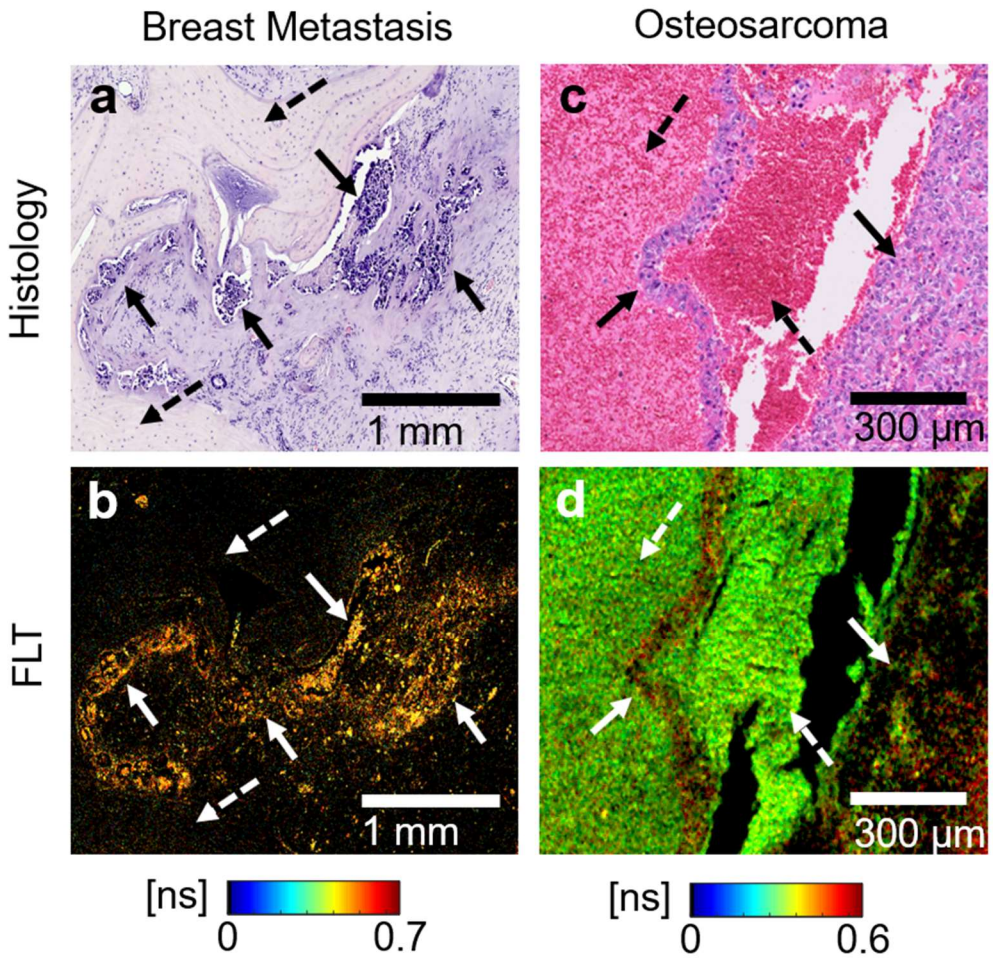

Fig. S2: **a**, Histology, and **b**, confocal FLIM images of a specimen collected from a patient with bone metastasis of breast cancer who was administered a flat dose of 50 mg ICG at the induction of anesthesia. **c**, Histology, and **d**, confocal FLIM images of a specimen collected from an osteosarcoma patient systemically injected with 75 mg ICG one day before surgery. For both tumor types, the cancer cell nests are indicated by solid arrows (**a** and **c**) that correspond to long ICG FLT (**b** and **d**). Normal bone is indicated by dashed arrows in (**a**) that did not show a detectable ICG uptake (**b**). In the osteosarcoma specimen (**c**), large hemorrhagic pools of red blood cells (dashed arrows) were observed that displayed higher ICG fluorescence, but shorter FLT compared to the nearby cancer cell nests.

Supplementary Table 3: Patient-level ROC curve analysis for the performance of FLT and fluorescence intensity in bone and soft tissue sarcoma

Patient ID	FLT			Intensity		
	Sensitivity	Specificity	AUC	Sensitivity	Specificity	AUC
P1	92.3	94.3	0.97	16.0	40.0	0.27
P2	94.9	94.4	0.98	87.0	63.6	0.78
P3	94.7	92.6	0.98	73.7	66.7	0.72
P4	96.0	96.4	0.99	8.0	40.0	0.08
P5	87.5	91.3	0.95	77.8	60.0	0.66
P6	96.9	95.3	0.97	75.0	45.9	0.55
P7	95.3	92.1	0.96	83.9	37.5	0.56
P8	96.1	90	0.97	79.8	60	0.73
Mean ± SD	94.2±3.0	93.3±2.2	97.1±1.3	62.7±31.6	51.7±12.1	54.4±24.7

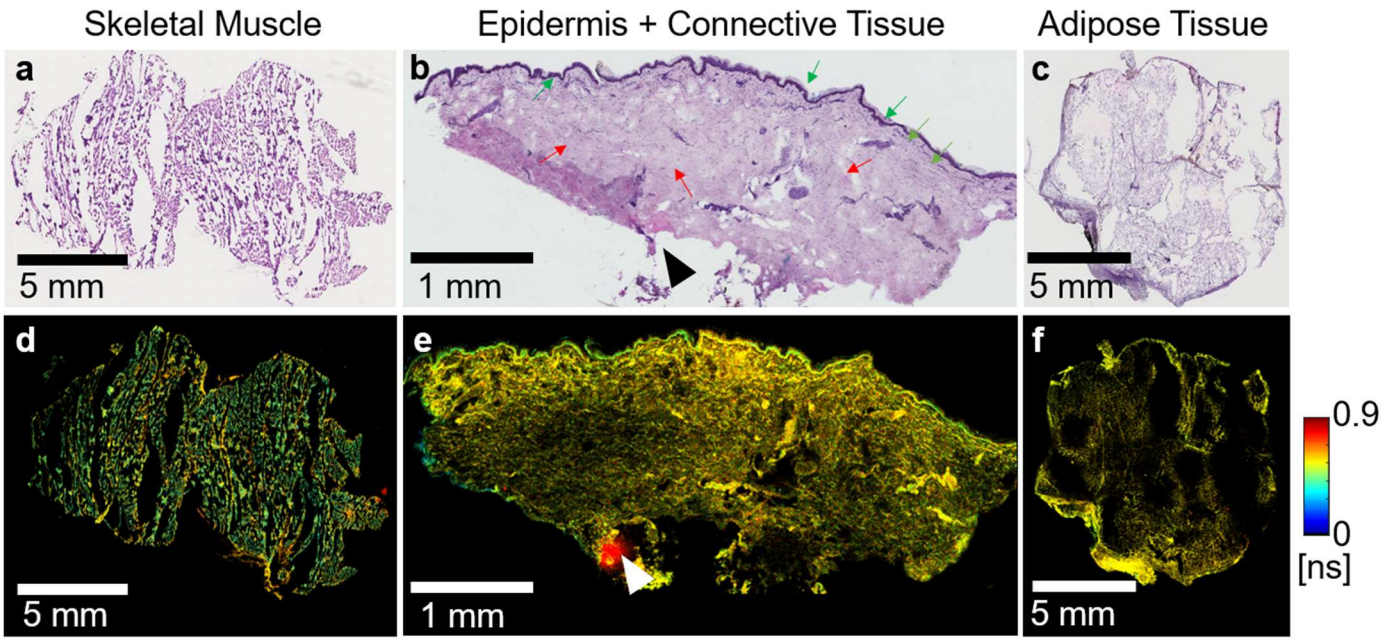

Fig. S3: Histology images of normal tissues, **a**, Skeletal muscle, **b**, epidermis with connective tissue, and **c**, adipose tissue obtained from a myxofibrosarcoma patient ~2 h after systemic administration of ICG (0.5 mg/kg). Fresh normal tissue specimens away from the primary tumor were collected immediately following surgery and inking. Tissues were frozen in OCT overnight and sectioned (10 μm thickness) for confocal FLIM and H&E staining. A significant amount of connective tissue (red arrows) can be seen along with the epidermis (green arrows) in (**b**). Confocal FLIM images of the same sections of **d**, skeletal muscle, **e**, epidermis with connective tissue, and **f**, adipose tissues are shown. ICG FLTs in skeletal muscle, skin, connective tissue, and adipose tissue were 0.42 ns ± 0.04 ns, 0.41 ns ± 0.02 ns, 0.45 ns ± 0.01 ns, and 0.44 ± 0.02 ns, respectively. The long FLT component indicated by the 'while arrowhead' in (**e**) was considered an image artifact since it was not associated with the tissue (black arrowhead in (**b**)).

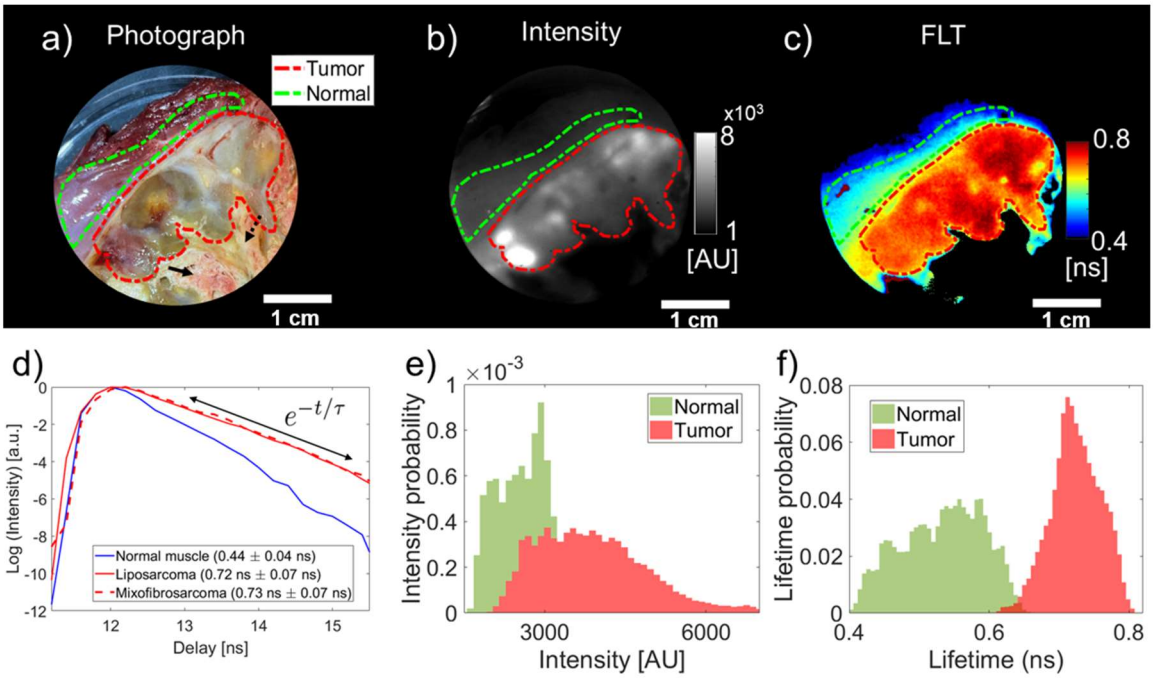

Fig. S4: **a**, Photograph of a fresh resection specimen from a patient with liposarcoma, 3 h after systemic ICG injection, showing clinically identified viable tumor (dashed red) and normal muscle (dashed green). Necrosis (solid arrow) and scar tissue (dotted arrow), formed due to extensive neo-adjuvant radiation therapy, are also visible in the FOV. **b**, Fluorescence intensity was highly heterogeneous within the tumor and significantly overlapped with the intensity of adjacent normal muscle, making it difficult to distinguish tumor from muscle. **c**, FLT maps clearly distinguished the tumor mass from normal muscle tissue. **d**, Representative wide-field TD fluorescence decay profiles of liposarcoma (red solid, 0.72±0.07 ns), myxofibrosarcoma (red dashed, 0.73±0.07 ns), and normal muscle (blue, 0.44±0.04 ns) outside the clinically identified tumor margin. **e,** Fluorescence intensity, and **f**, FLT histograms of tumor (red) and normal muscle tissue (green) identified from the photograph in (**a**) are shown. A high degree of overlap of fluorescence intensities between the tumor and normal tissue was observed, while the tumor FLTs were distinctly longer than the normal tissue FLTs with minimal overlap.

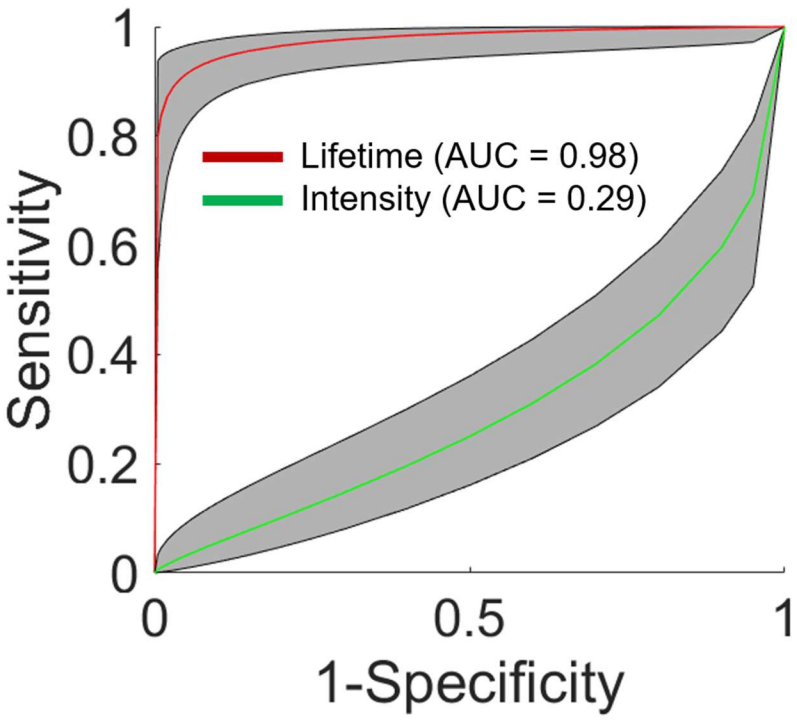

Fig. S5: ROC curve analysis of GBM specimens with low tumor density regions (< 20% tumor cells) as the histologically negative group, while the positive group consisted of moderate and high tumor density regions. Red: ROC curve for FLT, and Green: ROC curve for fluorescence intensity. Gray-shaded areas represent 95% CI. The ROC curve for FLT represents a sensitivity of 90.7% (95% CI – 83.3%-95%) and specificity of 97.5% (95% CI – 87.1%-99.6%). The ROC curve for fluorescence intensity represents a sensitivity of 47.1% (95% CI) and a specificity of 20% (95% CI).

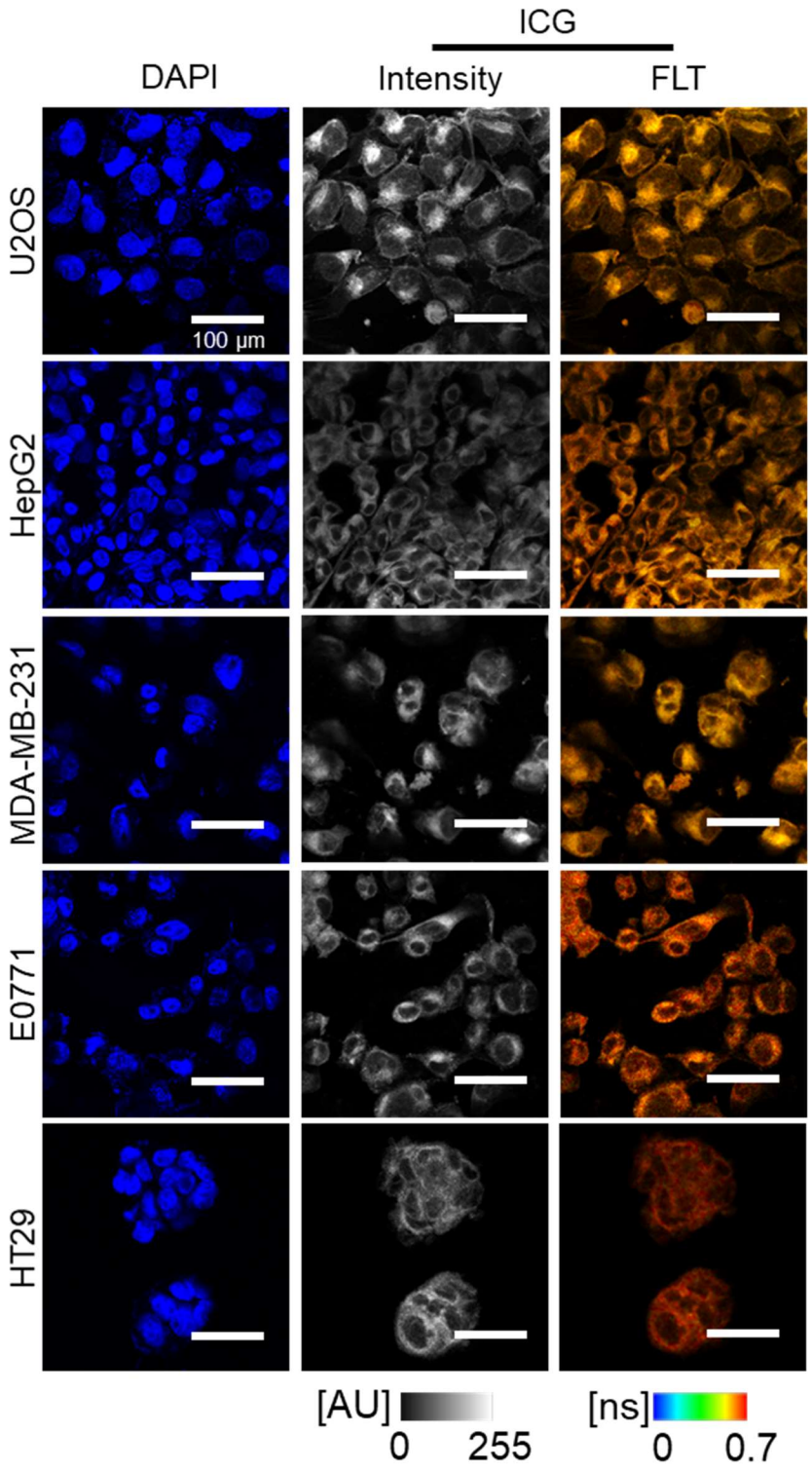

Fig. S6: Nuclear stain with DAPI (left), and ICG fluorescence images (intensity – center, FLT - right) for various cancer cell types are shown. The panel of cell lines explored includes osteosarcoma (U2OS), hepatocellular carcinoma (HepG2), colorectal adenocarcinoma (HT-29), and breast cancer (MDA-MB-231). All cell lines showed sufficient ICG uptake and the intracellular FLTs were consistently greater than 0.6 ns. Scale bar 100 µm.

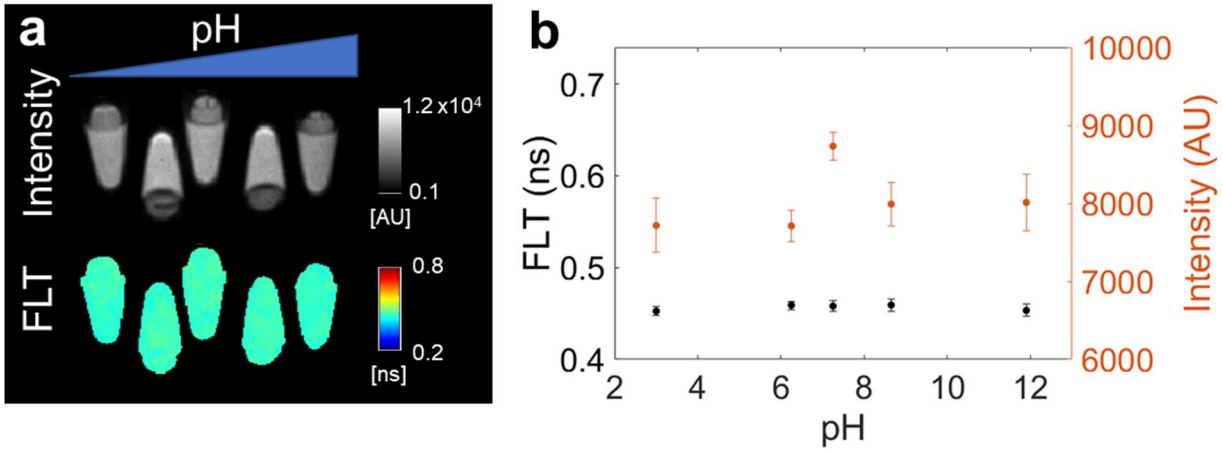

Fig. S7: The effects of solvent pH on ICG fluorescence properties were studied in vitro. **a**, Fluorescence intensity (top) and FLT (bottom) images of ICG PBS at increasing pH are shown. The pH of the solutions from left to right are 3, 6.25, 7.25, 8.65, and 11.9, respectively. **b**, Scatter plot of fluorescence intensity (red) and FLT (black) with increasing pH. Both fluorescence intensity and FLT of ICG remained unaffected by pH.

Supplementary Table 4: List of reagents

Material	Supplier
ICG	MGH Pharmacy
PBS	Thermo Fisher Scientific
0.25% Trypsin-EDTA	Thermo Fisher Scientific
High Glucose DMEM	Thermo Fisher Scientific
FBS	Thermo Fisher Scientific
Penicillin-Streptomycin	Thermo Fisher Scientific
Lab Tek 8-Well Chamber Slides	Thermo Fisher Scientific
MEBM Media Kit	Lonza
LysoTracker Deep Red	Invitrogen
Ethyl Alcohol	Sigma-Aldrich
Dexamethasone	Sigma-Aldrich
DMSO	Sigma-Aldrich
VECTASHIELD HardSet Antifade Mounting Media	VECTOR Laboratories
U2OS	ATCC
HT29	ATCC
HepG2	ATCC
MDA-MB-231	ATCC
MCF 10A	ATCC
PFA	Sigma-Aldrich
STELLARIS 8 FALCON	Leica
FFSMART-780	TOPTICA Photonics
Multimode Fiber	Thorlabs
835/70-nm Band-Pass Filter	AVR Optics
PicoStar Gated Intensifier	LaVision
acA5472-17um CMOS Camera	Basler
Leica CM1860 UV	Leica
Keyence BZ-X810 Microscope	Keyence
Plan Apo 10x/0.45 Objective	Nikon
MATLAB	MathWorks
ImageJ	NIH
Basler acA5472-17um CMOS Camera	Basler

Supplementary Table 5: FLT of ICG in varying viscosities

Viscosity (Cp)	1.005	1.31	1.76	3.72	10.8	22.5	35.5	60.1	109	219	523
30 mM ICG (µl)	5	5	5	5	5	5	5	5	5	5	5
Glycerol (µl)	0	10	20	40	60	70	75	80	85	90	95
PBS (µl)	95	85	75	55	35	25	20	15	10	5	0
FLT (ns)	0.29±0.02	0.29±0.04	0.29±0.03	0.36±0.004	0.39±0.01	0.46±0.02	0.48±0.01	0.56±0.03	0.63±0.03	0.71±0.04	0.74±0.02

Supplementary Table 6: FLT of ICG at increasing FBS concentration in DMEM

FBS (%)	0	0.1	1	5	10	20	30	50	100
DMEM (µl)	497.5	497	492.5	472.5	447.5	397.5	347.5	247.5	0
FBS (µl)	0	0.5	5	25	50	100	150	250	497.5
10mM ICG (µl)	2.5	2.5	2.5	2.5	2.5	2.5	2.5	2.5	2.5
FLT (ns)	0.32±0.01	0.33±0.01	0.46±0.01	0.62±0.02	0.72±0.02	0.78±0.02	0.83±0.02	0.86±0.02	0.85±0.01

Supplementary Table 7: FLT of varying concentrations of ICG in 10% FBS containing DMEM

ICG conc (µM)	10	20	40	100	200	400	1000
DMEM (µl)	449.5	449	448	445	440	420	400
FBS (µl)	50	50	50	50	50	50	50
10mM ICG (µl)	0.5	1	2	5	10	20	50
FLT (ns)	0.85±0.01	0.82±0.01	0.77±0.01	0.67±0.01	0.62±0.01	0.57±0.02	0.47±0.03

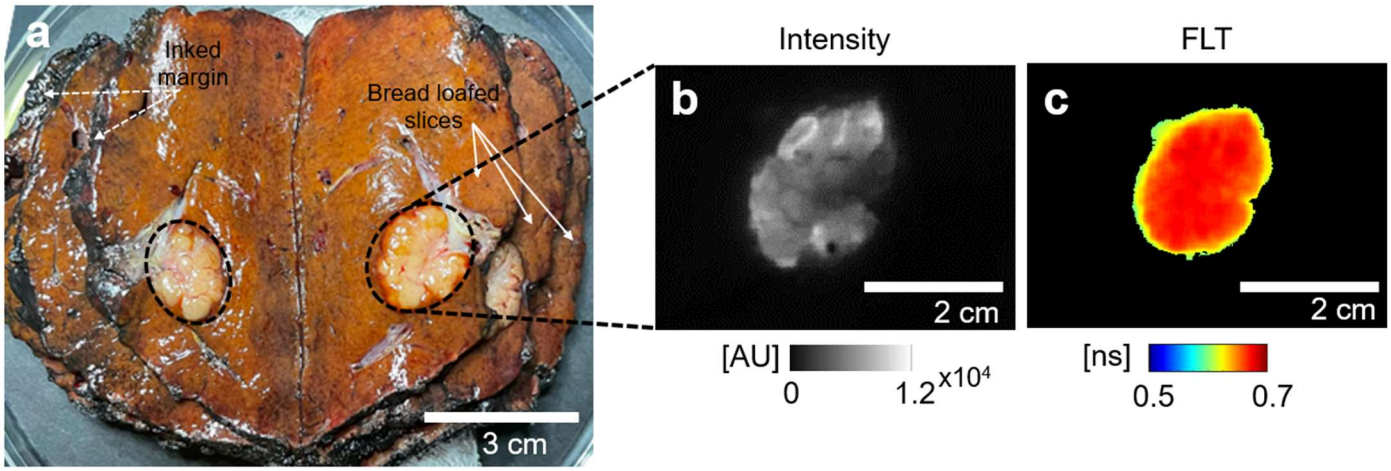

Fig. S8: **a**, Excised HCC tumor along with adjacent normal liver tissue after inking and bread loafing by the surgeon. The bread loafed slices are indicated by solid arrows and dashed arrows mark the inked margin. Each slice of the bread loaf is roughly 1 cm thick. The tumor is seen as areas of discoloration on either side of the sections (dashed outlines). **b**, Fluorescence intensity, and **c**, FLT images of the tumor from one of the bread loafed slices. While ICG uptake was mostly confined to the tumor, fluorescence intensity within the tumor was highly heterogeneous. However, a homogenously distributed long FLT was observed in the tumor.